

**Morphology and kinematics of Planetary Nebulae**  
**II. A Diabolo model for NGC 3132**

H. Monteiro<sup>1</sup>, C. Morisset<sup>1,2</sup>, R. Gruenwald<sup>1</sup>,  
and  
S. M. Viegas<sup>1</sup>

Received \_\_\_\_\_; accepted \_\_\_\_\_

---

<sup>1</sup>Instituto Astronômico e Geofísico, USP, Avenida Miguel Stefano, 4200 CEP  
04301-904 São Paulo, SP, Brazil

<sup>2</sup>Laboratoire d'Astronomie Spatiale, Traverse du Siphon, Les Trois Lucs,  
13012 Marseille, France

## ABSTRACT

We use a 3D photoionization modeling tool to study the morpho-kinematic properties of the Planetary Nebula (PN) NGC 3132. We show that it is possible to reproduce the low resolution observations (spectra and images) with an ellipsoidal shell. However, high resolution observations, as those showing a density variation along the nebula and the  $[\text{O III}]\lambda 5007$  velocity profiles, definitively rule out this description. We show that a bipolar Diabolo shape with a  $40^\circ$  rotation of the symmetry axis relative to the line of sight successfully reproduces the observed images, as well as the high resolution observations.

### 1. Introduction

The determination of the three-dimensional matter distribution in planetary nebulae is essential for a knowledge of the nebula ejection mechanism. A precise understanding of the nebula geometry which produces the observed morphology can also provide constraints on stellar evolution theories. The geometry and the density distribution of PNe are generally derived from line imaging, assuming that a surface brightness enhancement corresponds to a density enhancement. After a first descriptive study of the morphology of PNe (Curtis 1918), more detailed studies indicate two different interpretations for the observed morphology of these objects: a) the different observed morphologies are due to different projections of a same common basic structure (Minkowski & Osterbrock 1960, Khromov & Kohoutek 1968); b) the different types in which PNe can be classified (bipolar, elliptical, etc.) correspond to different evolutionary stages (Balick 1987). In this second approach, the morphology can also be related to the nebular and stellar properties, particularly the mass of the progenitor star (e.g. Peimbert & Torres-Peimbert 1983, Calvet & Peimbert 1983, Stanghellini, Corradi & Schwarz 1993, Corradi & Schwarz 1995). This point of view is corroborated by the studies of Zhang & Kwok (1998). These authors, assuming a three-dimensional ellipsoidal shell with density variations and a complete absorption of the ionizing photons, which are reconverted in H recombination photons, produce simulated radio and  $\text{H}\alpha$  images which are compared to the observations. The visual appearance of PNe were also compared with models obtained for ionization-bounded prolate shells by Masson (1990). Assuming an ellipsoidal shell with constant thickness and that the ionizing radiation is geometrically diluted, Masson (1990) compared theoretical and observed  $\text{H}\alpha$  images. However, a given emission line image results from the sum of line intensities along the line of sight. The exact location of the regions which produce each line depends on the gas density distribution, but also on

the ionization distribution, which, in turn, depends on the characteristics of the ionizing star and on the nebular gas abundance. Consequently, different emission lines provides information on different regions of the nebula, and only a consistent photoionization model applied to a realistic gas structure can give an accurate density distribution on the nebula.

In this paper we show that the geometry of a PN derived by fitting the observed image of a line emission and/or a line intensity ratio is misleading, since different geometries can reproduce the same observational data. Other constraints, coupled with a detailed 3D photoionization model, must be used for better defining the geometry, as illustrated by the planetary nebula NGC 3132.

Based on emission line imaging, an ellipsoidal geometry for NGC 3132 is assumed by various authors. Such a geometry is then suggested in a first approach. Studies similar to that of Masson (1990) using a prolate shell could explain the observed morphology of NGC 3132. Notice that the ellipsoidal shell model of Zhang & Kwok (1998) also reproduces the general trends of the observed  $\text{H}\alpha$  image of NGC 3132. Using a geometry defined by two concentric ellipsoids and a 3D photoionization code, Bässgen, Diesch & Grewing (1990, hereafter BDG90) fit the observed  $[\text{O III}]$  and  $[\text{N II}]$  line images, as well as the emission line spectra taken through four slits.

Spatio-kinematic models for NGC 3132 were proposed by Sahu & Desai (1986, hereafter SD86) to explain the observed asymmetric double-peaked  $[\text{O III}]\lambda 5007$  line profiles in five positions. SD86 assert that an ellipsoidal model with velocity and density asymmetries reproduces the observed expansion velocities and correctly explains the nature of the profile asymmetries. However, in their paper, only the fit to the line profile at the central position is shown. Line profiles, as a powerful tool for studying the nebula geometry, are discussed by Morisset, Gruenwald & Viegas (2000, hereafter MGV2000).

As it will be shown below, all the models assuming an ellipsoidal emitting shell lead to the same problems: neither can reproduce the low central density observed by SD86 and Juguet et al. (1988) nor the observed asymmetric double-peaked profiles in regions far from the center of the nebula. After a description of the available observations of NGC 3132 (§2), we show that ellipsoidal shell models do not reproduce all the available observations (§3). A “Diabolo” nebula successfully explaining all the main observational trends is presented in §4. The conclusions are outlined in §5.

### 2. Observational data for NGC 3132

A consistent photoionization model giving a realistic description of a PN has to account for all the observational

data coming from different types of observation. In the following, a summary of the data available for NGC 3132 is presented.

The logarithm of the observed  $H\beta$  flux ranges from -10.49 (Perek 1971) to -10.20 (Pottasch et al. 1977). The extinction  $E(B-V)$  is of the order of 0.1 (Pottasch et al. 1977, Mendez 1978, Feibelman 1982, Gathier, Pottasch & Pel 1986).

The calculated values for the Zanstra He II temperature of the ionizing star of NGC 3132 ranges from 73 000 K (de Freitas Pacheco, Codina & Viadana 1986) to 110 000 K (Pottasch 1996). Distance determinations indicate values from  $\sim 0.51$  kpc (de Freitas Pacheco et al. 1986, Pottasch 1996) to 1.63 kpc (Torres-Peimbert & Peimbert 1977). The ionizing star luminosity available in the literature is  $72 L_\odot$  (Mendez 1978) or  $\sim 125 L_\odot$  (Pottasch 1984).

HST/WFPC2 images for  $H\alpha$ ,  $[O\text{ I}]\lambda 6300$ ,  $[O\text{ III}]\lambda 5007$ ,  $[N\text{ II}]\lambda 6583$ , and  $[S\text{ II}]\lambda\lambda 6717,6731$  are available at the CADC server from the Trauger's proposal # 6221<sup>3</sup>. Lower resolution images and contours were obtained by Juguet et al. (1988), BDG90, Pascoli (1990), Condal et al. (1981), and Schwarz et al. (1992).

Spectroscopic observations of NGC 3132 can be found in Aller & Faulkner (1964), Kaler (1976), Torres-Peimbert & Peimbert (1977), and BDG90. Expansion velocities of  $14.7 \text{ km s}^{-1}$  for  $[O\text{ III}]\lambda 5007$  and  $21.0 \text{ km s}^{-1}$  for  $[O\text{ II}]\lambda\lambda 3726,3729$  were obtained by Meatheringham, Wood & Faulkner (1988), for slits along the major axis. High resolution spectra for  $[O\text{ III}]\lambda 5007$  in five positions were obtained by SD86, who also deduced a velocity of  $14 \text{ km s}^{-1}$  at the central position. The line profiles are all asymmetrical and double peaked. Since the observed red peak is more intense towards the center, the asymmetry can not be due to local absorption.

Electronic densities are generally obtained from the  $[O\text{ II}]$  or  $[S\text{ II}]$  line intensity ratios corresponding to intensities integrated on a slit. Torres-Peimbert & Peimbert (1977) obtained  $1000 \text{ cm}^{-3}$ , while Meatheringham et al. (1988) and Stanghellini & Kaler (1989) give, respectively,  $600 \text{ cm}^{-3}$  and  $430 \text{ cm}^{-3}$ . More detailed observations show a variation of the electronic density measured in different positions. Density determination by Juguet et al. (1988), from the  $[S\text{ II}]\lambda\lambda 6717,6731$  line intensity ratio, shows a double-peaked distribution along the NS direction, reaching up to  $1300 \text{ cm}^{-3}$  at the periphery of the nebula and decreasing to  $300 \text{ cm}^{-3}$  at the central position. Recent observations have confirmed this density distribution trend (Monteiro, Gruenwald & de Souza, in preparation). *It will be shown that the decrease in density at the central region is the key observation that rules out the description of NGC 3132 as*

*a geometrical ellipsoidal shell.*

### 3. The ellipsoidal model

The 3D photoionization code used in this paper is described in Gruenwald, Viegas & Broguière (1997). The output of the code is treated by IDL tools performing rotations, projections, and velocity profiles. A full description of these tools is given by MGV2000.

In order to fit the observed morphology of NGC 3132 ( $[O\text{ III}]\lambda 5007$  and  $[N\text{ II}]\lambda 6583$  line images), as well as the emission line spectra taken through 4 slits, BDG90 proposed a model obtained by a 3D photoionization code. The geometry and input parameters proposed by BDG90 are taken as a starting point for our 3D model of NGC 3132. Elements heavier than Ne were not included in BDG90 model. For S, Cl, and Ar we assumed a solar abundance (Grevesse & Anders 1989), while Mg, S, Cl, and Fe are depleted by one hundred (Stasinska & Tylenda 1986). Thus, the gas chemical abundance, in number, is: H: 1.0, He: 0.126, C: 7.1(-4), N: 2(-4), O: 6(-4), Ne: 8.2(-5), Mg: 3.8(-7), Si: 3.55(-7), S: 1.62(-5), Cl: 3.16(-7), Ar: 3.6(-6), Fe: 4.7(-7). The central ionizing radiation is a black-body of 90 000 K and  $150 L_\odot$ . The model consists of two prolate ellipsoids defining a shell and an inner cavity (the outer zone being empty). The inner ellipsoid has a semi-minor axis of  $1.27 \text{ } 10^{17} \text{ cm}$  and a semi-major axis of  $2.32 \text{ } 10^{17} \text{ cm}$ , while the outer one has  $1.96 \text{ } 10^{17} \text{ cm}$  and  $2.45 \text{ } 10^{17} \text{ cm}$ , respectively. The density in the inner cavity is constant ( $464 \text{ cm}^{-3}$ ). In BDG90, the shell density varies along the three directions. Here only the most important density gradient (along the major axis Z) is assumed. It varies from  $\sim 1200 \text{ cm}^{-3}$  at one pole to  $\sim 900 \text{ cm}^{-3}$  at the opposite pole. This gradient is needed in order to reproduce the observed asymmetrical brightness enhancement shown by the optical images.

The calculations are performed assuming the on-the-spot approximation (see MGV2000). Initially the cube containing  $1/8$  the nebula is divided in  $36^3$  cells. In order to improve the numerical resolution, some of these cells are subdivided, resulting in 133 000 cells. Once the calculations converged, the whole nebula is recovered (see MGV2000). Following BDG90, the images are obtained after a  $7^\circ.5$  rotation around the X axis (perpendicular to the line of sight).

#### 3.1. Matter- and Radiation-bound models

The results obtained by BDG90 for the line intensities are not reproduced by our ellipsoidal model. First, the geometrical thickness of the shell, adopted by these authors, is not large enough to absorb all the photons. Our model with the BDG90 geometry leads to a matter-bound (M-bound) nebula. The model is then unable to reproduce the observed  $[N\text{ I}]\lambda\lambda 5198,5200$  strong lines, characteristic of a

<sup>3</sup>Guest User, Canadian Astronomy Data Center, which is operated by the National Research Council, Herzberg Institute of Astrophysics, Dominion Astrophysical Observatory

radiation bound nebula. Notice that the measured intensity for  $[O\text{ I}]\lambda 6300$ ,  $\sim 0.3$  H $\beta$  (Torres-Peimbert & Peimbert 1977), also indicates that the nebula must be mainly radiation-bound (R-bound). Although the details of the BDG90 code are not available in their paper, the difference with our results may come from the optical depth calculation, which is the key-parameter determining the model. Models with a low number of cells (which implies too large cells) tend to overestimate the optical depth. In this case, for the same geometrical thickness, the model would be R-bound instead of M-bound. Our model has 40 times more cells than BDG90. This can explain why, using the same input parameters, our model is M-bound while theirs is R-bound. In order to have a R-bound shell, reproducing the observed low-ionization emission lines, the outer ellipsoid size must be increased by at least 20%. A second reason for the discrepancies between our model and that of BDG90 is the lack of elements heavier than Ne in their code, which leads to an underestimation of the cooling processes. In order to test this effect, a heavy-element free-BDG90 model was built. The  $[O\text{ III}]\lambda 5007$  and  $[N\text{ II}]\lambda 6583$  line intensities (relative to H $\beta$ ) increase, respectively, by 30% and 16%. This can partly explain the differences with BDG90 results, since the optical depth effect, discussed above, must be also important.

In the following, we will refer to the matter-bound model using the dimensions of BDG90 as the M-BDG90 model and to the 20% “extended” radiation-bound model as the R-BDG90 model. The results of both models are presented in Table 1. As expected, the stronger differences appear for the low ionization lines ( $[N\text{ I}]\lambda\lambda 5198, 5200$  and  $[O\text{ I}]\lambda 6300$ ). Nevertheless, even the R-BDG90 model is far from reproducing the results obtained by BDG90, as discussed below.

EDITOR: PLACE TABLE 1 HERE.

### 3.2. Ellipsoidal model results

The superposition of the  $[N\text{ II}]\lambda 6583$  HST image and the theoretical isophotes obtained from the R-BDG90 model is shown in Fig. 1. The shape is well reproduced, as well as the variation of the surface brightness along the major axis. To adjust the modeled shape and dimensions to the observed ones, a reduction of 4% in the distance used by BDG90 (670 pc) is necessary. Note that this new value for the distance is in the range of the calculated distances to NGC 3132 (§2).

For a comparison of our results with the observations of Juguet et al. (1988), the theoretical N-S density distribution is calculated from the theoretical  $[S\text{ II}]\lambda\lambda 6717, 6731$  ratio (using the Alexander & Balick 1997 fit) for a 4” width slit, centered on the nebula. As seen from Fig. 2, this

model assuming an ellipsoidal geometry (dashed line) does not reproduce the observed central decrease in density.

In order to obtain the theoretical  $[O\text{ III}]\lambda 5007$  emission line profiles, a radial velocity law  $\vec{V} = \alpha \vec{r}/r + \beta \vec{r}$  is used. Three possible sets of  $\alpha$  and  $\beta$  values are assumed:  $\alpha = 14.7, 9.1, 0$  km s $^{-1}$  and  $\beta = 0, 9.1/r_o, 23.8/r_o$  km s $^{-1}$  cm $^{-1}$ , respectively. The normalization factor,  $r_o = 3 \cdot 10^{17}$  cm, is of the order of the size of the nebula. The  $\langle V \rangle_{5007}$  and  $\langle V \rangle_{3726}$  emission line mean velocities for the whole nebula (as defined in MGV2000) are given in Table 2. For the three sets of values defining the velocity law, the parameters were chosen in order to give  $\langle V \rangle_{5007} = 14.7$  km s $^{-1}$ , as obtained from the observed profile reported by Meatheringham et al. (1988). The corresponding theoretical  $\langle V \rangle_{3726}$  mean velocity depends on the parameters  $\alpha$  and  $\beta$  and is always slightly lower than the observed value (21 km s $^{-1}$ ). The five positions at which the  $[O\text{ III}]\lambda 5007$  line profiles were observed are shown in SD86 (their Fig. 1a) superposed on an U-band image (Kohoutek & Lausten 1977). The calculated velocity profiles for  $[O\text{ III}]\lambda 5007$  are shown in Fig. 3. Since the three sets of parameters of the adopted velocity law give similar line profiles, only the results for the  $\alpha = 9.1$  km s $^{-1}$  and  $\beta = 9.1/r_o$  km s $^{-1}$  cm $^{-1}$  law is shown. In the upper-right panel the aperture is shifted from the center by 2.8” NE. This shift corresponds to the pointing accuracy of the telescope used by SD86 and it allows to check if the effect of the pointing precision on the profile is important. The central double peak is reproduced. However, the observed asymmetry can only be obtained if the nebula is tilted by about 30°, whereas the results shown in Fig. 3 were obtained assuming a rotation angle of 7°.5, as proposed by BDG90. The observed double peaks at the four external positions are not reproduced. Note that the observed profiles were taken by SD86 at positions where the U band emission is strongest. In the U band, the nebular emission is dominated by the  $[O\text{ II}]\lambda 3726$  line, so the observations were taken at the extreme outer part of the nebula. Thus, the radial velocity at these positions is quasi-perpendicular to the line of sight and an apparent velocity of  $\sim 10$  km s $^{-1}$  would require an unrealistic high radial velocity.

EDITOR: PLACE TABLE 2 HERE.

Finally, a simple way to verify the inadequacy of the ellipsoidal model in reproducing the density gradient and the low ionization lines is the following: let us consider a dense shell ( $\sim 1000$  cm $^{-3}$ ) with a geometrical thickness  $t$  and radius  $R$ , around a less dense cavity ( $\sim 300$  cm $^{-3}$ ). The line emissivity is proportional to the square of the density. Thus, in order to reproduce the observed density distribution, the main contribution to the central emission must come from the low density gas, implying  $t < 0.02R$ . Such a thin shell will have a total emissivity far below the observed one, and will

be matter-bound, not producing the low ionization lines. A radiation-bound model, necessary to explain the low ionization lines cannot reproduce the density gradient as shown above. This rules out the description of NGC 3132 as a *closed ellipsoidal shell*. An ellipsoidal shell with a hole just aligned to the central line of sight could be proposed, but such an *ad hoc* geometry seems unrealistic.

From all the results presented above we conclude that an ellipsoidal model for NGC 3132 is not appropriate to explain the observational data. Thus, a new model is proposed below.

#### 4. The Diabolo model

PNe imaging suggests that several objects can have a “Diabolo” shape (e.g. Hour-Glass nebula and NGC 2346). In order to reproduce this shape, we adopt a two-zone gas distribution, illustrated in Fig. 4: a) a dense zone (with a density of  $1300 \text{ cm}^{-3}$ ) defined by the intersection of two spheres of the same radius ( $3 \cdot 10^{17} \text{ cm}$ ) but with centers shifted by  $10^{17} \text{ cm}$ , defining the “Diabolo-shape”, and b) a low-density gas,  $300 \text{ cm}^{-3}$ , filling the rest of the nebula. The shadowing in the figure is just used to give a better 3D visualization and does not correspond to a density variation. The model was calculated for  $1/8$  of the nebula and the whole nebula was reconstructed in a  $10^6$  cells cube. We keep the chemical abundances and ionizing star characteristics of BDG90 model (§3). No attempt to adjust these parameters were made in order to improve the fit of the emission line ratios. In fact, the scope of this paper is just to show that a strong constraint on the geometry is the density distribution. Once this distribution is reproduced, other observed features, unexplained by previous models, can also be explained.

##### 4.1. The Diabolo model results

The effect of varying the angle of view of the nebula is shown in Fig. 5. Practically all the observed regular morphologies of PNe are reproduced: from a clearly butterfly image (axis of symmetry perpendicular to the line of sight) to a well round nebula (axis of symmetry aligned to the line of sight) through an ellipsoidal one. With an appropriate orientation of  $40^\circ$  relative to the line of sight, the observed optical shape of NGC 3132 (ellipsoidal shape) can be reproduced. As said above (§1), such feature can also be reproduced by the ellipsoidal shell model of Zhang & Kwok (1998), as well as by a model similar to that of Masson (1990). However, these models are not self-consistent with respect to the ionization balance and, as will be shown below, other constraints will rule out an ellipsoidal model for this nebula.

With a Diabolo morphology the contribution from the

dense region to the central emission is reduced, helping to solve the close ellipsoidal shell problems. At the same time, the projected velocity of the gas in the external parts of the nebula will be high enough, reproducing the observed double peak, as shown below.

Regarding the emission line ratios, the results of the Diabolo model (fourth column of Table 1) are similar to those obtained from the R-BDG90 model. In addition, HST line images in  $\text{H}\beta$ ,  $[\text{O III}]\lambda 5007$ ,  $[\text{N II}]\lambda 6583$  and  $[\text{O I}]\lambda 6300$  are shown Fig. 6 (four upper panels) and can be compared to the corresponding Diabolo model images (four lower panels). The observed ellipsoidal shape is well reproduced, as well as the ionization stratification. The brightness asymmetry along the major axis is not reproduced by the adopted axi-symmetrical model of the nebula. Such asymmetry could be explained either by a density gradient or an ionization source that is not in the geometrical center of the Diabolo.

The electronic density distribution obtained from the  $[\text{S II}]\lambda\lambda 6717,6731$  ratio is also shown in Fig. 2 (solid line). *The observed decrease of the density (§2) in the central part of the nebula is reproduced.* This and the line profiles discussed below are the main improvements obtained by the Diabolo shape.

The same velocity laws applied for the R-BDG90 model are used (§3.2) with  $r_o = 5 \cdot 10^{17} \text{ cm}$ . The three different  $[\text{O III}]\lambda 5007$  profiles obtained with the three sets of parameters of the velocity law are shown in Fig. 7 and can be compared to the observations (SD86). The profiles show the double peaks at the six positions, *a feature not reproduced by the ellipsoidal shell model*. The asymmetry is well reproduced at the four external positions. The asymmetry at the central position is not reproduced, as long as an axisymmetric nebula is used, even considering a shift of  $2.8''$  as shown in the upper right panel. Notice that at the central position only the low density gas contributes to the emission. Thus, any asymmetry in the velocity field and/or in the low density distribution will lead to the observed asymmetry, requiring no change in the higher density distribution associated to the Diabolo shape.

The three sets of parameters for the velocity law were chosen in order to obtain the same  $\langle V \rangle_{5007}$  ( $14.7 \text{ km s}^{-1}$ , Table 2; the results for  $\langle V \rangle_{3726}$  remain the same as for the R-BDG90 models); however, for  $\alpha = 0$  (dashed lines), the peaks of the observed profiles at the central part of the nebula occur for a lower velocity (Fig. 7, upper panels). Furthermore, in this case, the velocity law does not reproduce the observed profiles since one of the peaks is almost nonexistent. The results obtained with the other two sets of parameters (solid and dot-dashed lines) are very similar. Nevertheless, for  $\alpha \neq 0$  and  $\beta \neq 0$ ,  $\langle V \rangle_{3726}$  is higher than  $\langle V \rangle_{5007}$ , approaching the observed result (Table 2) of Meatheringham et al. (1988).

## 5. Concluding remarks

We have shown in this paper that the lack of high resolution observations (spatial and spectroscopic) may lead to a wrong conclusion about the morphology of a PN.

A new modeling tool based on a 3D photoionization code is used to consistently reproduce all the available observations of NGC 3132. Using an ellipsoidal geometry, all the low resolution observations (flux, emission line spectrum, imaging) could be reproduced. However, neither the density variations indicated by the  $[S\,II]\lambda\lambda6717,6731$  ratio, nor the  $[O\,III]\lambda5007$  velocity profiles could be explained by such a model. To account for these observations, a drastic change in the geometry of the nebula is necessary. The proposed Diabolo shape offers the solution to the density distribution, as well as to the asymmetric double-peaked emission line profiles, while also explaining the low resolution observations.

A Diabolo shape may reproduce the observed bipolar morphology of many PNe. In fact, Bryce, Balick & Meaburn (1994) suggested that NGC 6720 is not a spherical expanding shell as often assumed, but must be bipolar in nature, since the observed [NII] emission line profiles are split in two components. A bipolar shape emerges from studies of the formation and evolution of PNe, in particular those related to the interacting wind model (Kwok, Purton, & Fitzgerald 1978). Recent hydrodynamical models (e.g. Dwarkadas, Chevalier & Blondin 1996; Mellema 1997) suggest that a Diabolo type shape can be produced in the accepted scenario of PNe formation (post AGB envelope ejection with wind interaction). In fact, recent high resolution images taken with the Hubble Space Telescope show that PNe with this type of structure is not uncommon. Some nice examples are the Hour-Glass nebula, NGC 2346, NGC 6537 and Hb-5.

No attempt was made to fine tuning the emission line ratios. This can be achieved through changes in the ionizing star characteristics, in the chemical abundances, as well as through small adjustments in the density distribution, which will not change the main conclusions of this paper, in particular the Diabolo shape. Furthermore, in the models presented here, the ionizing source is assumed to be at the center of symmetry of the nebula. However, there are evidences that the star should be shifted by  $\sim 1.7''$  from the geometrical center of the nebula (Kohoutek & Lausten 1977 and SD86). A model accounting for this out-of-center ionizing star may still improve the results, leading to a better agreement with the observations regarding the brightness asymmetry and the emission line profile at the central position.

We have shown here the importance of a 3D photoionization model, combined with imaging results and also with high resolution observations, to impose relevant constraints on the PN geometry. The misclassification of NGC 3132 as an ellipsoidal PN instead of a bipolar one casts doubts on

the statistical results correlating the morphology and other PNe properties, such as abundances or progenitor type.

The authors would like to thank the referee, Dr. Sun Kwok, for his valuable comments and suggestions. C. Morisset is thankful to IAGUSP for the hospitality during his post-doctoral visit. This work was supported by CNPq (n. 304077/77-1, n. 306122/88-0, and n. 150162/96-0), FAPESP (n. 97/13428-4 and n. 98/01922-7), and PRONEX/FINEP (n. 41.96.0908.00).

## REFERENCES

Alexander, J. & Balick, B. 1997, AJ, 114, 713  
 Aller, L. H., & Faulkner, D. J. 1964, IAU Symp. 20, 45  
 Balick, B. 1987, AJ, 94, 671  
 Bässgen, M., Diesch, C. & Grewing, M. 1990, BDG90, A&A 237, 201  
 Bryce, M., Balick, B. & Meaburn, J. 1994, MNRAS, 266, 721  
 Calvet, N., & Peimbert, M. 1983, Rev. Mexicana Astron. Astrofis., 5, 319  
 Condal, A., Pritchett, C., Fahlman, G.G. & Walker, G.A.H. 1981, PASP, 93, 695  
 Corradi, R. L. M. & Schwarz, H. E. 1995, A&A, 293, 871  
 Curtis, H. D. 1918, Pub. Lick Obs. 13, 55  
 Dwarkadas, V. V., Chevalier, R. A. & Blondin, J. M. 1996, ApJ, 457, 773  
 Feibelman, W. A. 1982, AJ, 87, 555  
 de Freitas Pacheco, J. A., Codina, S. J. & Viadana, L. 1986, MNRAS, 220, 107  
 Gathier, R., Pottasch, S. R. & Pel, J. W. 1986, A&A, 157, 171  
 Grevesse, N. & Anders, E. 1989, American Institute of Physics Conference Series, 183, 1  
 Gruenwald, R., Viegas, S. M. & Broguière, D. 1997, ApJ, 480, 283  
 Juguet, J. L., Louise, R., Macron, A. & Pascoli, G. 1988, A&A, 205, 267  
 Kaler, J. B. 1976, ApJS, 31, 517  
 Khromov, G. S. & Kohoutek, L. 1968, IAU Symp. 34, Planetary Nebulae (Dordrecht: Reidel), 227  
 Kohoutek, L. & Lausten, S. 1977, A&A, 61, 761  
 Kwok, S., Purton, C. R. & Fitzgerald, P. M. 1978, ApJ, 219, L125  
 Masson, C. R. 1990, ApJ, 348, 580

Meatheringham, S. J., Wood, P. R. & Faulkner, D. J. 1988, *ApJ*, 334, 862

Mellema, G. 1997, *A&A*, 321, L29

Minkowski, R. & Osterbrock, D. E. 1960, *ApJ*, 131, 537

Mendez, R. H. 1978, *MNRAS*, 185, 647

Morisset, C., Gruenwald, R. & Viegas, S. M. 2000, MGV2000, *ApJ*, submitted

Pascoli, G. 1990, *AAS*, 83, 27

Peimbert, M., & Torres-Peimbert, S. 1983, *IAU Symp.* 103, *Planetary Nebulae* (Dordrecht: Kluwer), 233

Perek, L. 1971, *Bulletin of the Astronomical Institutes of Czechoslovakia*, 22, 103

Pottasch, S. R., Wesselius, P. R., Wu, C. -C. & Van Duinen, R. J. 1977, *A&A*, 54, 435

Pottash 1984, *Planetary Nebulae*, Reidel, Dordrecht

Pottasch, S. R. 1996, *A&A*, 307, 561

Sahu, K. C. & Desai, J. N. 1986, SD86, *A&A*, 161, 357

Schwarz, H. E., Corradi, R. L. M. & Melnick, J. 1992, *A&AS*, 96, 23

Stanghellini, L., Corradi, R. L. M., & Schwarz, H. E. 1993, *A&A*, 279, 521

Stanghellini, L. & Kaler, J. B. 1989, 343, 811

Stasinska, G. & Tylenda, R. 1986, *A&A*, 155, 137

Torres-Peimbert, S. & Peimbert, M. 1977, *Revista Mexicana de Astronomia y Astrofisica*, 2, 181

Zhang, C.Y. & Kwok, S. 1998, *ApJS*, 117, 341

Fig. 1.— Superposition of the HST and the theoretical images of [N II] $\lambda\lambda$ 6548, 6583. The theoretical results correspond to the R-BDG90 model.

Fig. 2.— N $\leftrightarrow$ S variation of [S II] $\lambda\lambda$ 6717, 6731 density from the R-BDG90 model (dashed line) and from the Diabolo model (solid line).

Fig. 3.— [O III] $\lambda\lambda$ 5007 velocity profiles obtained from the R-BDG90 model. The positions and the size aperture are the same as in SD86 (their Fig. 2). In the upper-right panel the aperture is shifted from the center by 2.8" (see text).

Fig. 4.— Gas distribution for the Diabolo model. Only the denser zone ( $1300 \text{ cm}^{-3}$ ) is shown.

Fig. 5.— H $\beta$  images from the Diabolo model. From the upper-left to the lower-right panel the angle between the axis of symmetry and the sky plane increases by  $10^\circ$  from  $0^\circ$  to  $80^\circ$ .

Fig. 6.— The top panels correspond to HST images of NGC 3132 while the bottom panels to the Diabolo model.

Fig. 7.— [O III] $\lambda\lambda$ 5007 velocity profiles for the Diabolo model using the velocity law  $\vec{V} = \alpha \cdot \vec{r}/r + \beta \cdot \vec{r}$ , with  $r_0 = 310^{17} \text{ cm}$ , and  $(\alpha, \beta) = (14.7, 0)$ ,  $(9.1, 9.1/r_0)$ , and  $(0, 23.8/r_0)$  are shown, respectively, by dashed, solid, and dot-dashed lines.

Table 1: Emission line intensities relative to H $\beta$

Line Å	M-BDG90	R-BDG90	Diabolo
[O III] $\lambda$ 4363	0.022	0.018	0.013
He II $\lambda$ 4686	0.085	0.059	0.065
[O III] $\lambda$ 5007	6.045	4.700	3.690
[N I] $\lambda$ 5200	0.010	0.159	0.200
He I $\lambda$ 5876	0.175	0.189	0.190
[O I] $\lambda$ 6300	0.037	0.320	0.353
[N II] $\lambda$ 6583	2.792	5.090	5.337
[S II] $\lambda$ 6717	0.193	0.689	0.825
[S II] $\lambda$ 6731	0.236	0.745	0.846
H $\alpha$	2.904	2.915	2.917
H $\beta$ <sup>1</sup>	6.553	9.651	9.050

<sup>1</sup> In  $10^{-11}$  erg cm $^{-2}$  s $^{-1}$ , for a distance of 670 pc.

Table 2: Mean line velocities for the adopted velocity law

$\alpha^a$	$\beta^b$	$\langle V \rangle_{5007}^a$	$\langle V \rangle_{3726}^a$
14.7	0.	14.7	14.7
9.1	9.1	14.7	15.9
0.	23.8	14.7	17.8

<sup>a</sup> in km s $^{-1}$

<sup>b</sup> in km s $^{-1}$ /r<sub>0</sub>, with r<sub>0</sub> = 310<sup>17</sup> cm for the R-BDG90 model and r<sub>0</sub> = 510<sup>17</sup> cm for the Diabolo model

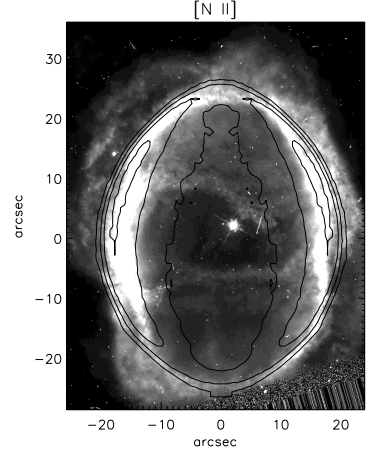


Fig. 1.—

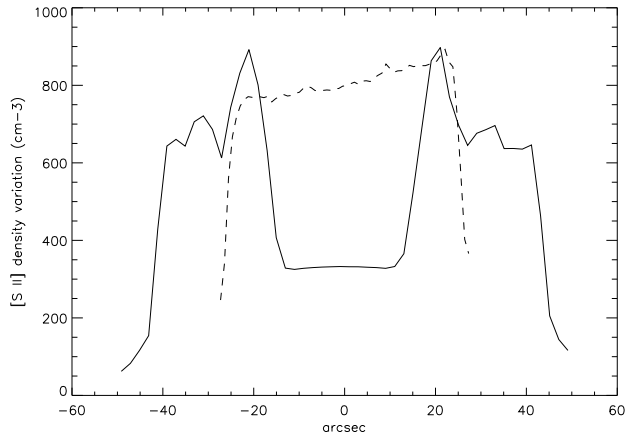


Fig. 2.—

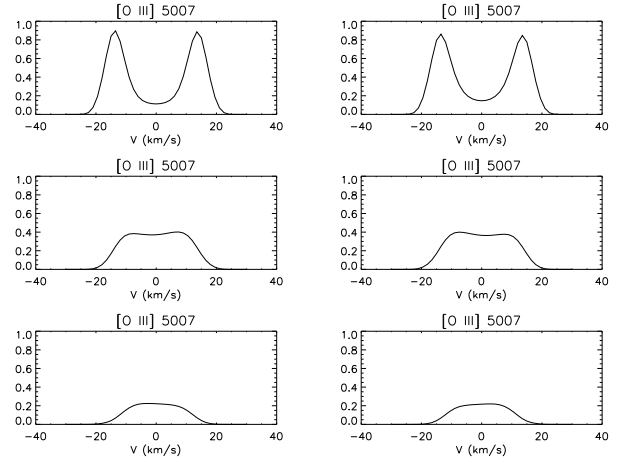


Fig. 3.—

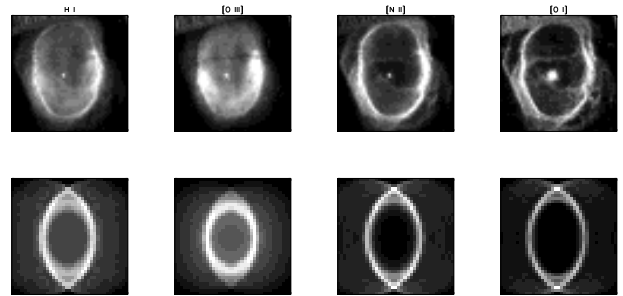
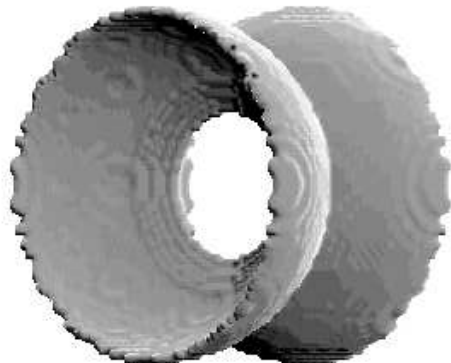


Fig. 6.—

Fig. 4.—

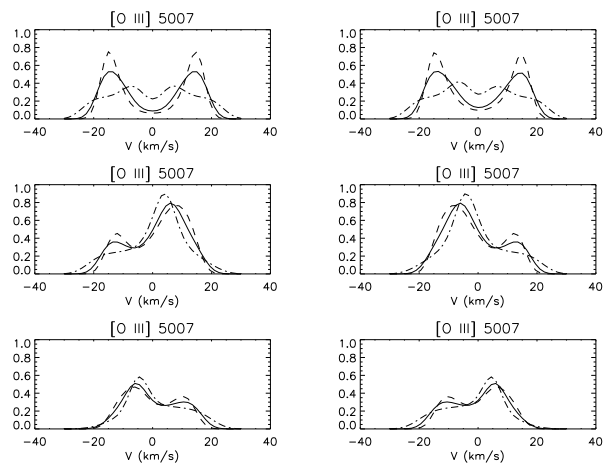
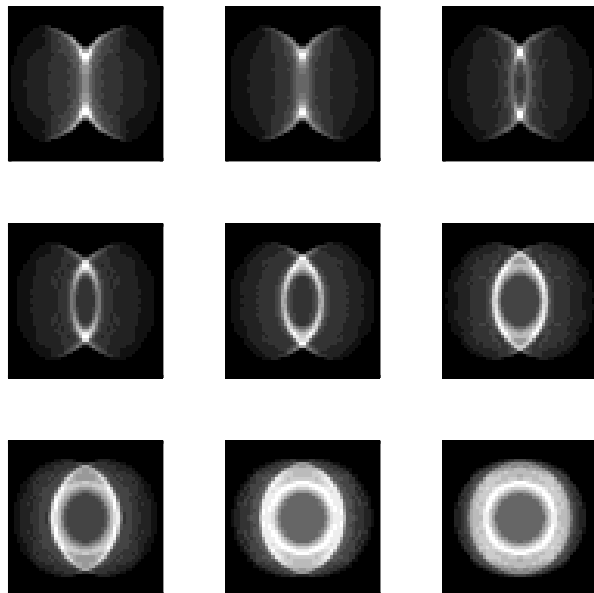


Fig. 7.—

Fig. 5.—